Confidence in predicted position error explains saccadic decisions during pursuit

Jonathan D Coutinho[1], Philippe Lefèvre[2,3], Gunnar Blohm[1]

1. Centre for Neuroscience Studies, Queen's University
2. Institute of Information and Communication Technologies, Electronics and Applied Mathematics (ICTEAM)), Université catholique de Louvain
3. Institute of Neuroscience (IoNS), Université catholique de Louvain

Keywords: decision making, confidence, saccade, pursuit, Bayesian, prediction

Abstract

The coordination between continuously-controlled and discretely-initiated orienting movements is a fundamental problem in motor control. This coordination is vital for maintaining high-acuity vision of moving objects, which requires foveating the object's image through continuous smooth pursuit and discretely triggered saccadic eye movements. However, the decision mechanism underlying this coordination remains inadequately characterized. During these coordinated eye movements, pursuit is rapidly initiated by retinal image velocity while intervening saccades are triggered with highly variable latency contingent on both retinal image velocity and position. Here we propose a new computational strategy simulating the decision mechanism triggering saccades during pursuit. In this model, future position error and its associated uncertainty are predicted through Bayesian inference across noisy, delayed sensory observations of retinal image motion. This probabilistic prediction of position error enables the computation of the confidence that a saccade will be needed, triggering saccades upon accumulating confidence to a threshold. Saccade confidence corresponds to the relative certainty that the image is positioned outside the fovea (quantified through log probability ratio). This model predicts the occurrence and latency distributions of saccades across a range of step-ramp target trajectories and externally imposed sensory uncertainty levels (e.g. via Gaussian blurring of the visual target). We suggest this stochastic, predictive decision making process represents a fundamental principle for the neural coordination of movement.

Introduction

The coordination of continuous and discrete reorienting is a fundamental problem in neuroscience. This is further complicated by the inevitability of noise and delays in sensory observations (Faisal et al., 2008; van Beers et al., 2002). The oculomotor system has promising potential for investigating this motor coordination problem due to the relative simplicity in modelling the biomechanics of eye motion and the wealth of existing data concerning the underlying neurophysiology driving eye movements (Van Gompel et al., 2007). When viewing objects in motion, the oculomotor system coordinates two types of eye movements to reorient and actively stabilize a visual image onto the fovea (the region of the retina with the highest visual acuity). The first type of eye movement, saccades, are discretely triggered to rapidly reposition a visual image onto the fovea (Goffart, 2009). The second type, smooth pursuit, is continuously deployed to minimize the motion of a visual image on the retina (Keller and Heinen, 1991; Krauzlis, 2004). The oculomotor system judiciously coordinates if and when saccades are needed during pursuit, triggering spatially accurate saccades despite sensorimotor noise and delays (Orban de Xivry and Lefèvre, 2007; Quinet and Goffart, 2015). This decision process is also stochastic (Carpenter and Reddi, 2001; Ratcliff, 2001; Wolpert and Landy, 2012), resulting in trial-by-trial variability in the timing of saccades during pursuit (de Brouwer et al., 2002a). However, a quantitative explanation of the mechanism underlying this predictive, stochastic decision process remains poorly characterized. Studying oculomotor coordination of saccades during pursuit has the potential to provide general insights into decision making in motor coordination.

Previous studies have investigated how visual sensory signals correlate with saccade trigger during pursuit initiation and maintenance, finding that both visual position and velocity errors are important in this motor decision (Bieg et al., 2015; de Brouwer et al., 2002b, 2002a; Rashbass, 1961). To investigate the sensory basis of saccadic decision making during pursuit,

experimentalists commonly employ a paradigm involving an abrupt change in target position and velocity (named step-ramp trajectories after their appearance on a position-time plot). It has been well established that the probability of saccade occurrence is minimized during pursuit initiation if the change in position and velocity are in opposite directions and balanced in magnitude such that the target recrosses the initial fixation position in 200 ms (Rashbass, 1961). Target trajectories that recross the fixation position after a slightly longer or shorter duration tend to evoke an intermediate probability of saccade occurrence with highly variable latency (Bieg et al., 2015). Similarly during pursuit maintenance, it was observed that the ratio between position and velocity error correlates well with the occurrence of saccades and roughly correlates with saccade latency (de Brouwer et al., 2002b). This parameter was originally coined as eye-crossing time, but henceforth referred to as time-to-foveation to parallel the time-to-collision parameter in studies of steering control (Regan and Gray, 2000) and the time-to-contact parameter in studies of limb control and interception (Chang and Jazayeri, 2018; Tresilian, 1995). While time-to-foveation is a useful behavioural correlate, it remains unsuitable as a decision variable due to its instability as velocity errors approach zero (time-to-foveation goes to infinity) and its inability to address how sensory noise is accommodated. Furthermore, the concept of time-to-foveation is based on the linear extrapolation and intersection of the eye and target trajectory which do not necessarily intersect in two-dimensional tracking. Thus, while existing datasets have catalogued saccadic decision making during pursuit, an underlying decision mechanism has not yet been proposed.

Probabilistic inference through sequential sampling has provided a successful framework for decision making under uncertainty, particularly in studies of perceptual decision making (Gold and Shadlen, 2001; Hanks and Summerfield, 2017) but less often applied to oculomotor control. In this framework, noisy evidence is sequentially sampled and linearly integrated until a fixed threshold is reached, terminating the decision process and triggering a

response. Choices, response times, and neuronal responses in sensorimotor decision areas are consistent with this framework (Gold and Shadlen, 2007; Schall, 2001, 2000). Recently, an innovative stochastic model of pursuit was developed where noisy, delayed sensory signals are probabilistically estimated through Kalman filtering (Orban de Xivry et al., 2013). Their model allows for the closed-loop simulation of probabilistic visual motion estimation and pursuit dynamics, which opens the possibility to model the probabilistic sensory basis of stochastic saccadic decision making during pursuit.

To model the saccade trigger mechanism, we propose a decision process that accumulates evidence that a saccade is needed (saccade confidence) to a threshold. We define saccade confidence as the log probability ratio of the probability of the target being left vs right of the foveal center. This definition has roots in the sequential probability ratio test (Forstmann et al., 2016; Wald and Wolfowitz, 1948) and agrees with the proposition that the term confidence should reflect the probability that a decision/response is correct/appropriate given the observed evidence (Pouget et al., 2016). Modelling the decision variable triggering saccades with this definition of confidence allows small, low-uncertainty position errors to trigger saccades when sustained, while large, high-uncertainty position errors may fail to trigger saccades when transient. The model can simulate saccade latency distributions evoked by a range of step-ramp target trajectories matching human behavioural data (Bieg et al., 2015; de Brouwer et al., 2002b) and illustrates how predictive mechanisms can flexibly coordinate continuous and discrete reorienting movements. We suggest this stochastic, predictive decision mechanism represents a fundamental principle in the neural control of motor coordination.

Methods

Global Model Overview

The purpose of this model is to explain how catch-up saccades are triggered during smooth pursuit. We extend an existing Bayesian model of sensory motion estimation and smooth pursuit dynamics (Orban de Xivry et al., 2013) to develop a model of the decision mechanism triggering saccades. The model consists of three interconnected modules: a sensory pathway employing Kalman filtering for state estimation, a decision pathway employing bounded accumulation of saccade confidence and a motor pathway implementing the dynamics of pursuit and (simplified) saccades (Figure 1). An important addition to the sensory pathway of the model was the inclusion of linear motion extrapolation (Figure 1; Sensory Extrapolation) to update retinal state estimates, compensating for sensorimotor delays. We assume that the goal of a saccade is to reorient a visual image to a preferred retinal location, presumably the fovea (which defines the zero-position in our retinotopic coordinate system). The saccade decision mechanism relies on the probabilistic, predictive position error estimate to compute the log-probability ratio that the image is outside the fovea (which we define as saccade confidence). A saccade is triggered when saccade confidence is temporally accumulated to a threshold value. We use this model to simulate the occurrence and latency distributions of saccades during pursuit initiation and steady-state pursuit evoked by step-ramp target trajectories.

Sensory Pathway

The sensory pathway is an extension of the visual motion processing pathway previously described (Orban de Xivry et al., 2013). We denote matrices in bolded uppercase, vectors in bolded lowercase, and scalars in regular lowercase. The true retinal image state, $\boldsymbol{\delta}^{det}$, is defined as the difference between the position, velocity, and acceleration of the target, $\boldsymbol{t}$, and the eye, **e**:

$$\boldsymbol{\delta}_{\boldsymbol{k}}^{det} = \boldsymbol{t}_{\boldsymbol{k}} - \boldsymbol{e}_{\boldsymbol{k}} \tag{1}$$

$$\boldsymbol{\delta_k^{det}} = \begin{bmatrix} PE_k^{det} \\ RS_k^{det} \\ RA_k^{det} \end{bmatrix} \tag{2}$$

where PE is Position Error, RS is Retinal Slip, RA is Retinal Acceleration and k represents the current discrete time step in the numerical simulation.

The observed retinal state is delayed by 70 ms (Krauzlis and Lisberger, 1994; Tavassoli and Ringach, 2009) and corrupted by additive and signal-dependent noise:

$$\boldsymbol{\delta_k^{obs}} = \boldsymbol{\delta_{k-70}^{det}} + \boldsymbol{\phi_{mult}}\boldsymbol{\delta_{k-70}^{det}} + \boldsymbol{\varphi_{add}} \tag{3}$$

where $\boldsymbol{\phi_{mult}}$ and $\boldsymbol{\varphi_{add}}$ are uncorrelated noise covariance matrices with values drawn at each time step, k, from $\boldsymbol{\phi_{mult}} \sim N(0, \boldsymbol{\sigma_{mult}^2})$ and $\boldsymbol{\varphi_{add}} \sim N(0, \boldsymbol{\sigma_{add}^2})$. These terms represent the signal-dependent and baseline levels of noise corrupting visual sensory information. Both behavioural analyses and electrophysiological recordings in the superior colliculus (encoding position error) and the middle temporal area (encoding retinal slip and acceleration) suggest that the information in visual signals driving saccades and pursuit are consistent with signal-dependent noise constraints (*saccades:* Sparks, 1986; Harris and Wolpert, 1998, 2006; van Beers, 2007; Goossens and van Opstal, 2012*; pursuit:* Maunsell and Van Essen, 1983; Lisberger and Westbrook, 1985; Nover et al., 2005; Osborne et al., 2005, 2007; Stein et al., 2005; Osborne and Lisberger, 2009).

Using the delayed, noisy observations of image motion, a Bayes-optimal probabilistic estimate of image motion, $\boldsymbol{\hat{\delta}^{sens}}$, is computed through Kalman filtering (Kalman and Bucy, 1961). This method of recursive Bayesian estimation combines noisy observations with priors of the noise characteristics and dynamics of the world (ie: a generative model) to estimate retinal state. The generative model contains information about the expected evolution of retinal motion, as well as the noise characteristics that map the underlying state into a noisy observation. In

this generative model, the components of retinal state are assumed to be uncorrelated and thus it is expected that the evolution of retinal state can be described by a random walk:

$$\boldsymbol{\delta}_{\boldsymbol{k+1}}^{\boldsymbol{sens}} = \boldsymbol{\delta}_{\boldsymbol{k}}^{\boldsymbol{sens}} + \boldsymbol{\lambda}_{\boldsymbol{k}} \tag{4}$$

where $\boldsymbol{\lambda}_{\boldsymbol{k}}$ is an uncorrelated, additive process noise with $\boldsymbol{\lambda}_{\boldsymbol{k}} \sim N(0, \boldsymbol{Q}^{\boldsymbol{2}})$ representing the state variability, a prior belief about how retinal state changes over time. The generative model also contains knowledge that the observed image motion at time k, $\boldsymbol{\delta}_{\boldsymbol{k}}^{\boldsymbol{obs}}$, represents a noisy version of the retinal state, $\boldsymbol{\delta}_{\boldsymbol{k}}^{\boldsymbol{sens}}$ (Equation 5).

$$\boldsymbol{\delta}_{\boldsymbol{k}}^{\boldsymbol{obs}} = \boldsymbol{\delta}_{\boldsymbol{k-70}}^{\boldsymbol{sens}} + \boldsymbol{\gamma}_{\boldsymbol{k}} \boldsymbol{\delta}_{\boldsymbol{k-70}}^{\boldsymbol{sens}} + \boldsymbol{\upsilon}_{\boldsymbol{k}} \tag{5}$$

where $\boldsymbol{\gamma}_{\boldsymbol{k}}$ and $\boldsymbol{\upsilon}_{\boldsymbol{k}}$ are the expected, uncorrelated signal-dependent and additive noises covariance matrices with $\boldsymbol{\gamma}_{\boldsymbol{k}} \sim N(0, \boldsymbol{D}^{\boldsymbol{2}})$ and $\boldsymbol{\upsilon}_{\boldsymbol{k}} \sim N(0, \boldsymbol{R}^{\boldsymbol{2}})$. These terms represent the brain's estimate of the signal-dependent and baseline levels of noise corrupting sensory observations. For each component of $\boldsymbol{\delta}$, we set $\boldsymbol{D}^{\boldsymbol{2}} = \boldsymbol{\sigma}_{\boldsymbol{mult}}^{\boldsymbol{2}}$ and $\boldsymbol{R}^{\boldsymbol{2}} = \boldsymbol{\sigma}_{\boldsymbol{add}}^{\boldsymbol{2}}$. Thus, we set the internal estimates of sensory noise parameters (D^2, R^2) to accurately reflect the actual sensory noise ($\boldsymbol{\sigma}_{\boldsymbol{mult}}^{\boldsymbol{2}}, \boldsymbol{\sigma}_{\boldsymbol{add}}^{\boldsymbol{2}}$), though an exact knowledge of these noise parameters is not crucial (Beck et al., 2012; Orban de Xivry et al., 2013).

The operation of the Kalman filter combines the current estimate of retinal state, $\widehat{\boldsymbol{\delta}}_{\boldsymbol{k}}^{\boldsymbol{sens}}$, the current noisy observation, $\boldsymbol{\delta}_{\boldsymbol{k}}^{\boldsymbol{obs}}$, and prior knowledge of the noise characteristics, ($\boldsymbol{Q}, \boldsymbol{R}, \boldsymbol{D}, \boldsymbol{\Omega}$), to optimally estimate image motion at the next time step, $\widehat{\boldsymbol{\delta}}_{\boldsymbol{k+1}}^{\boldsymbol{sens}}$ (Izawa et al., 2008; Todorov, 2005) (Equations 6-8).

$$\widehat{\boldsymbol{\delta}}_{\boldsymbol{k+1}}^{\boldsymbol{sens}} = \widehat{\boldsymbol{\delta}}_{\boldsymbol{k}}^{\boldsymbol{sens}} + \boldsymbol{K}_{\boldsymbol{k}}\left(\boldsymbol{\delta}_{\boldsymbol{k}}^{\boldsymbol{obs}} - \widehat{\boldsymbol{\delta}}_{\boldsymbol{k}}^{\boldsymbol{sens}}\right) + \boldsymbol{\eta}_{\boldsymbol{k}} \tag{6}$$

$$\boldsymbol{K}_{\boldsymbol{k}} = \boldsymbol{\Sigma}_{\boldsymbol{k}}^{\boldsymbol{sens}} \left(\boldsymbol{\Sigma}_{\boldsymbol{k}}^{\boldsymbol{sens}} + \boldsymbol{R}^{\boldsymbol{2}} + \boldsymbol{D}^{\boldsymbol{2}} \left(\boldsymbol{\Sigma}_{\boldsymbol{k}}^{\boldsymbol{sens}} + \widehat{\boldsymbol{\delta}}_{\boldsymbol{k}}^{\boldsymbol{sens}} \widehat{\boldsymbol{\delta}}_{\boldsymbol{k}}^{\boldsymbol{sens}^T}\right) \boldsymbol{D}^{\boldsymbol{2}^{\boldsymbol{T}}}\right)^{-1} \tag{7}$$

$$\boldsymbol{\Sigma}_{\boldsymbol{k+1}}^{\boldsymbol{sens}} = \boldsymbol{Q}^{\boldsymbol{2}} + \boldsymbol{\Omega}^{\boldsymbol{2}} + (\boldsymbol{I} - \boldsymbol{K}_{\boldsymbol{k}}) \boldsymbol{\Sigma}_{\boldsymbol{k}}^{\boldsymbol{sens}} \tag{8}$$

where $\boldsymbol{\varepsilon}_{\boldsymbol{k}}^{\boldsymbol{sens}}$ is the estimated error covariance, $\boldsymbol{I}$ is the identity matrix, and $\boldsymbol{\eta}_{\boldsymbol{k}}$ is the internal noise of estimation with $\boldsymbol{\eta}_{\boldsymbol{k}} \sim N(0, \Omega^2)$, which represents noise in the computations estimating the retinal state. The values of Kalman filter parameters are listed in Table 1.

In the final stage of the sensory pathway, extrapolation, the components of estimated image motion driving the pursuit and saccade motor pathways are updated based on their expected rate of change and knowledge of the delays inherent to each respective sensorimotor loop. This allows for compensation of sensorimotor delays. It has been shown that catch-up saccades can accurately foveate moving targets at saccade offset, effectively predicting changes in position error due to retinal slip accruing during visuomotor delays and saccade duration (de Brouwer et al., 2001; Guan et al., 2005; Price et al., 2005; Quinet and Goffart, 2015). Similarly it has been shown that both pursuit behaviour and motion-tuned neuronal activity in the middle temporal area of macaques account for target acceleration (Bennett et al., 2007; Krauzlis and Lisberger, 1994; Lisberger and Westbrook, 1985). It is not clear if target acceleration is also accounted in saccadic motor system (Bennett et al., 2007), and although it has been shown that position error can weakly drive smooth pursuit (Blohm et al., 2005), neither of these interactions were modelled in this study. Thus, in our model, position error was extrapolated $(\widehat{PE}^{pred})$ based on retinal slip $(\widehat{RS}^{sens})$, and retinal slip was extrapolated $(\widehat{RS}^{pred})$ based on retinal acceleration $(\widehat{RA}^{sens})$ to drive the saccadic and pursuit pathways respectively:

$$\widehat{PE}_k^{pred} = \widehat{PE}^{sens} + (T_{sacc})\widehat{RS}^{sens} \tag{9}$$

$$\Sigma_k^{PEpred} = \Sigma_k^{PEsens} + (T_{sacc})^2 \Sigma_k^{RSsens} \tag{10}$$

$$\widehat{RS}_k^{pred} = \widehat{RS}^{sens} + (T_{purs})\widehat{RA}^{sens} \tag{11}$$

$$\Sigma_k^{RSpred} = \Sigma_k^{RSsens} + (T_{purs})^2 \Sigma_k^{RAsens} \tag{12}$$

where $T_{sacc} = 130\ ms$ and $T_{purs} = 70\ ms$ represent the time duration of extrapolation for each respective signal. The rationale for the longer extrapolation duration for saccades is to account for the additional decision accumulation time, motor delay, and movement duration unique to the saccadic system.

Saccade Decision Pathway

The saccade decision pathway is inspired by the sequential probability ratio test and stochastic bounded accumulation models of decision making (Gold and Shadlen, 2007; Wald and Wolfowitz, 1948). This pathway computes saccade confidence and triggers saccades upon accumulating to a threshold. The first stage of this pathway reflects the probability of the image being right vs left of the foveal center using the predictive probabilistic estimate of position error:

$$P_k^{Right} = 1 - P_k^{Left} = \int_0^{+\infty} \frac{1}{\sqrt{2\pi\sigma^2}} e^{-\frac{\left(x-\widehat{PE}_k^{pred}\right)^2}{2\varepsilon_k^{PEpred}}} dx \tag{13}$$

where *x* represents a variable of spatial integration. Recall that the estimated position error value used in this computation is a predictive estimate accounting for retinal slip.

The next stage is the computation and leaky temporal accumulation of saccade confidence $(\hat{C})$, defined as the logarithm of the ratio between the above probabilities:

$$\hat{C}_k^{Right} = -\hat{C}_k^{Left} = \hat{C}_{k-1}^{Right} + \left(\frac{dt}{\tau_s}\right)\left(\log\left(\frac{P_k^{Right}}{P_k^{Left}}\right) - \hat{C}_{k-1}^{Right}\right) + \omega_k \tag{14}$$

where τ_s is the leakiness time constant, with $\tau_s = 25$ ms and ω_k is an uncorrelated noise term in the decision process with $\omega_k \sim N(0, 0.1^2)$. This estimate of saccade confidence acts as a decision variable that upon threshold crossing triggers a saccade (with an additional motor delay of 40 ms). For example, a rightward saccade is executed after $\hat{C}_k^{Right} > \theta_{saccade}$ with a 40 ms motor delay, where $\theta_{saccade} = 4.2$. While outside the focus of this investigation, a simple model of

saccade dynamics (described below) and saccade refractory period (200 ms) were implemented to illustrate how this saccade decision model can be implemented within a global framework for oculomotor control.

Pursuit Motor Pathway

The pursuit motor pathway transforms the predicted retinal slip, $\widehat{RS}_k^{pred}$, into an eye velocity command that is sent to the premotor system and eye plant. It is adapted from the image velocity motion pathway and positive efferent copy feedback loop used by previous models (Krauzlis and Lisberger, 1994; Krauzlis and Miles, 1996; Orban de Xivry et al., 2013). This pathway transforms predicted retinal slip into a command for eye motion, E. The pathway (Figure 2, top left) contains a linear function (G) to modify the RS input into an eye acceleration command, a second-order filter (H to adjust the time course of inputs, and a variable gain element (A). The parameters were similar to Krauzlis and Lisberger, 1994; Orban de Xivry et al., 2013.

$$G = 7 \tag{15}$$

$$H(s) = \frac{35^2}{s^2 + (2)(0.8)(35)s + 35^2} \tag{16}$$

$$A = 0.9 + \zeta_{trial} \tag{17}$$

where *s* represents the Laplace variable, and $\zeta_{trial} \sim N\left(0, \sigma_{purs}^2\right)$, with $\sigma_{purs}^2 = 0.05$. The purpose of this noise term is to simulate the trial-by-trial variability in pursuit gain observed in human behavioural responses and thus capture a realistic level of pursuit variability.

The output of this image velocity motion pathway was sent to a leaky integrator with positive feedback. The leaky integrator is characterized by a single time constant, $\tau_p = 100\, ms$,

that maintains eye velocity when $\widehat{RS}_k^{pred} = 0$. The positive feedback loop contains a linear gain element, $\frac{1}{\tau_p}$.

Saccade Motor Pathway

After saccade confidence reaches decision threshold, the saccade motor pathway (Figure 2, Saccade Motor Pathway) transforms a desired saccade amplitude, $\widehat{PE}_k^{pred}$, into an eye velocity command that is sent to the premotor system and eye plant. It should be noted that the purpose of this saccade model was not to exactly reproduce all aspects saccade dynamics, but rather to embed a model of saccade execution within our global framework. A motor delay of 40 ms was implemented between the time of saccade confidence threshold crossing and the execution of the saccade. The model of saccade dynamics is adapted from the local feedback model and bilateral burst neuron discharge rate pulse generator (Figure 2, PG) used by (Blohm et al., 2006; Jürgens et al., 1981; Scudder, 1988). In this pathway, the desired saccade amplitude is compared against an internal estimate of executed eye movement through negative feedback from a resettable integrator (Figure 2, RI), providing an estimate of motor error. This motor error is sent to a pulse generator, providing a saccadic motor command sent to the premotor system and eye plant. The pulse generator was based on the bilateral burst neuron discharge rate proposed by (Van Gisbergen et al., 1981):

$$y = \begin{cases} -b_m\left(1 - e^{\frac{x-e_0}{b_k}}\right) & if\ x < e_0 \\ b_m\left(e^{\frac{x-e_0}{b_k}} - e^{\frac{-x-e_0}{b_k}}\right) & if -e_0 < x < e_0 \\ b_m\left(1 - e^{\frac{-x-e_0}{b_k}}\right) & if\ x > e_0 \end{cases} \tag{18}$$

where the input, x, is motor error and the output, y, is a saccadic velocity command approximating the main sequence relationship between saccade amplitude, peak velocity, and

duration (Bahill et al., 1975). The parameters used match Blohm et al., 2006 (ie: $e_0 = 1$ deg; $b_m = 600$ deg/s; and $b_k = 3$ deg).

Final Common Motor Pathway

Eye velocity commands from the pursuit and saccade pathways are linearly added then sent through the premotor system to the eye plant. The premotor system consists of the sum of the motor command (with $gain = T_1 = 170\ ms$) and its integral; producing the pulse-step innervation pattern required to displace the eye and maintain eccentricity (Robinson, 1973). The eye plant is modelled as an overdamped, second-order system with time constants $T_1 = 170$ ms and $T_2 = 13$ ms. No additional motor noise was added to the eye plant, as the moment-by-moment variability in sensory observations and trial-by-trial variability in pursuit gain that we implemented provides a sufficiently realistic distribution of motor variability (Hu et al., 2007; Osborne, 2011; Osborne et al., 2005).

Simulations

The model was numerically simulated in MATLAB R2017a (Mathworks, Natick, MA, USA) using 1 ms discrete time steps. We simulated eye movements in response to step-ramp target motions selected to reproduce behavioural investigations of pursuit initiation (Bieg et al., 2015) and pursuit maintenance (de Brouwer et al., 2002b). For pursuit initiation, we simulated target steps between 1 to 12 degrees in one-degree increments, target velocities of ±10 deg/s and ±20 deg/s, and 100 repetitions at each step-ramp condition. For pursuit maintenance, the initial step-ramp was selected to recross the initial fixation position in 200 ms, thus minimizing initial saccade occurrence. The step sizes used were 2, 4, and 6 degrees with velocity changes of 10, 20, and 30 deg/s respectively in the opposite direction. The second step-ramp was selected using steps ranging from -20 to 20 degrees in increments of 2 degrees and velocity changes from -50 to 50 deg/s in increments of 10 deg/s, with 50 repetitions per double step-

ramp condition. Simulations of increased sensory noise were implemented using the same double step-ramp conditions while modifying the variance of the additive and multiplicative noise in position estimation to $2^2\ deg^2$ and 1.5^2 respectively. We analyzed the latency of the first occurring saccade after each step-ramp. Latency was determined using a 500 deg/s^2 acceleration criterion on the simulated eye trace.

Results

The model of oculomotor coordination presented here relies on Bayesian estimation of stochastic sensory signals and bounded accumulation of saccade confidence to trigger saccades during pursuit for foveal stabilization of a moving visual target. Since the framework driving pursuit movements employed here has been previously described (Orban de Xivry et al., 2013), we will focus our description on the saccade decision and trigger pathway. The notable novelty in this model is the computation of saccade confidence from probabilistic estimates of predicted retinal state. We define saccade confidence as the log-probability ratio that the image position is outside the fovea. In this model, saccades are triggered when temporally accumulated saccade confidence reaches a constant threshold.

Computation of Saccade Confidence

The computation of saccade confidence transforms a probabilistic prediction of position error into the log-probability ratio of the target being right vs left of the foveal center, which is then temporally leaky integrated. This process is schematically illustrated in Figure 3, where a constant estimate of predicted PE is used to compute saccade confidence without decision noise. Figure 3A illustrates the probability density function for an estimated PE of 2 degrees with low uncertainty (blue) and high uncertainty (red). The probability of the target being right (left) of the fovea is the area under the probability distribution to the right (left) of zero (denoted in black

dashed line). Saccade confidence is calculated by leaky integrating the ratio between these probabilities. Figure 3C illustrates the temporal evolution of saccade confidence based on the corresponding estimates of predicted PE. With low magnitude PE estimates, the saccade decision process is highly sensitive to the estimated uncertainty. Figures 3B illustrates an estimated position error of 5 degrees with low uncertainty (blue) and high uncertainty (red). Figure 3D demonstrates that at large magnitude PE estimates, the temporal evolution of saccade confidence is similar despite the difference in uncertainty. Thus, the estimation of saccade confidence accounts for both predicted PE and its uncertainty, but this computation is more sensitive to uncertainty for targets closer to the fovea.

Decision Process during Pursuit Initiation

To understand how sensory image motion drives saccadic decision making, Figure 4 illustrates examples of single trial simulations of oculomotor responses to two different trajectories of step-ramp target motion known to evoke and minimize saccade occurrence during pursuit initiation (red and blue, respectively) compared to a step trajectory (grey) (Figure 4A). These step-ramp target trajectories contain an abrupt, simultaneous position displacement and constant velocity shift that can be independently controlled by the experimenter. This paradigm is commonly used to investigate saccadic decision making during pursuit because it allows the experimenter to precisely control the retinal motion subsequent to the step-ramp onset (Bieg et al., 2015; de Brouwer et al., 2002a, 2002b; Rashbass, 1961).

In our model, noisy and delayed sensory observations are estimated through Kalman filtering (Figure 4B, 4C). To compensate for sensory delays, predictive retinal image state estimates are computed by extrapolating sensory estimates according to their first derivative and estimated delay (e.g. PE is updated by RS, figure 4D). This predictive PE estimate is then used to compute saccade confidence, which triggers saccades upon temporal leaky accumulation to a threshold (Figure 4E). Due to Kalman filtering, noisier signals (e.g. RS

compared to PE) require more time for accurate estimation, which is comparable to behavioural data suggesting an asynchronous influence of RS compared to PE in saccade programming (Schreiber et al., 2006). Thus, the observation that saccade latency is longer than pursuit latency is explained in the model by an additional temporal accumulator in the saccade decision pathway, allowing time for accurate RS information to accrue and influence the saccadic decision. Thus, estimated RS can either enhance or attenuate the evolution of saccade confidence by updating the current PE estimate away from or towards the fovea, leading to a reduction in saccade latency or a suppression of saccade execution respectively.

We simulated oculomotor responses across a range of step-ramp trajectories then calculated the proportion of saccadic trials and mean saccade latency. This model captures the major trends of behavioural data, predicting a minimization of saccade occurrence for targets whose trajectories recross the initial fixation position in about 200ms (Rashbass, 1961), as well as saccades with long latency for target trajectories slightly outside this recrossing time (compare with Figure 2 from Bieg et al., 2015). However, the behavioural data from Bieg et al., 2015 shows small differences in saccade latency for target motion away from the fovea vs towards the fovea at large step sizes that was not captured in this model. Overall, the model reproduces the major trends in saccade occurrence and latency variability responses during visually guided pursuit initiation.

Decision Process during Steady State Pursuit

The model was used to simulate steady state pursuit using target trajectories with an initial step-ramp designed to minimize saccades followed by a second step-ramp to test saccadic decision making. An example of single trial simulations is illustrated in Figure 6, which contrasts smooth and saccadic pursuit in response to two different double step-ramp target trajectories. Consistent with saccadic decisions during pursuit initiation, RS estimates leading to

an updating of PE towards foveal positions minimizes saccade confidence and subsequent saccade occurrence.

Across a range of double step-ramp target trajectories, we found that the sensory conditions preceding saccade trigger in simulations were highly comparable to human behavioural data. Figure 7 plots the values of RS and PE preceding each saccade trigger in simulations (left) and behavioural data (right). The region of this plot with very few saccade occurrences is described by de Brouwer and colleagues (2002b) as the smooth zone. The slope of the lines delimiting the smooth zone correspond to time-to-foveation values, demonstrating that the model emergently simulates similar correlations between time-to-foveation and saccade occurrence as human behaviour. Furthermore, the model simulated saccades of unusually long latency occurring when time-to-foveation was slightly outside this range (Figure 8). Thus, the model also explains saccadic decisions following a step-ramp perturbation during maintained pursuit.

New Model Predictions

A novel prediction from modelling results suggests that the absolute value of velocity change also correlates with saccade occurrence and latency beyond the relationship described by the time-to-foveation parameter. As the absolute value of the velocity change increases, the range of time-to-foveation values resulting in smooth trials tends to decrease (Figure 8). Since pursuit acceleration saturates at large values, larger velocity changes require longer acceleration durations, allowing more position error to accrue and thus increases the probability of saccade occurrence. Therefore, increasing the change in target velocity for a given time-to-foveation value will promote saccade occurrence.

A second novel prediction from this model is that increasing position uncertainty will impact saccade decision making during pursuit. Increasing position noise can be achieved

experimentally through Gaussian blurring of the pursuit target and implemented in the model through an increase of the noise corrupting sensory observations. Specifically, we predict a decrease in saccade occurrence and an increase in the variability of saccade latency in response to step-ramp target trajectories with time-to-foveation near the smooth zone, but a minimal impact on saccade latency distributions for negative time-to-foveation trajectories (corresponding to a position step and velocity change in the same direction) (Figure 9, top row). This is because the smooth zone corresponds to retinal motion where RS updates PE closer to the fovea and the saccade confidence is highly sensitive to sensory uncertainty for foveal image position estimates (Figure 3). Thus, increasing sensory uncertainty should lead to a larger range of tolerable position error estimates that fail to trigger saccades.

Discussion

We have developed a model of the saccade decision mechanism during visually guided pursuit in which saccade confidence (defined as the log-probability ratio of position error to the right vs left of the fovea) is computed from predictive estimates of position error and temporally accumulated to trigger saccades upon threshold crossing. This decision mechanism reproduces the Rashbass paradigm, where saccades occurrence during pursuit initiation is minimized if the target recrosses the initial fixation position in 200 ms (Bieg et al., 2015; Rashbass, 1961). The model also reproduces the behavioural observation that saccade occurrence is minimized when the time-to-foveation following a step-ramp during steady-state pursuit is between 40 and 180 ms and qualitatively reproduces the distribution of long-latency saccades evoked by step-ramps in and around this time-to-foveation range (de Brouwer et al., 2002b). Additionally, the model makes the novel prediction that for the same time-to-foveation value, saccades occur more frequently and with shorter latency with increasing target velocity. The model also predicts that increasing position uncertainty will increase the range of tolerable position errors that fail to

trigger saccades. Thus, the model provides a generalizable explanation for saccadic decisions during pursuit while fitting harmoniously within existing oculomotor models.

Model Limitations

The scope of this model is limited by only considering visual sensory inputs and omitting the influence of cognitive factors. For example, it has been shown that spatial attention is preferentially allocated ahead of tracking during pursuit (Chen et al., 2017; Khan et al., 2010). This could decrease the precision of sensory observations in unattended locations (Poletti et al., 2017), leading to a slower rise in saccade confidence and longer saccade latencies. This effect may underlie the differences in latency between forward and reverse saccades at large step sizes observed by Bieg et al., 2015. The allocation of attention also has more direct influences on saccade trigger (Kowler et al., 1995; Zhao et al., 2012), likely through influencing normative decision thresholds (Lo and Wang, 2006). Thus, cognitive factors likely modulate model parameters describing sensory noise and decision thresholds through mechanisms beyond the scope of this study, but the model accounts for the basic principles underlying these visually guided saccadic decisions.

Another important factor in human behavioural responses that was omitted in the model was mechanisms of learning and adaptation. This could also play a role in the differences between simulated results and Bieg et al., 2015. Since their paradigm only tested a single target speed for each individual it is conceivable that subjects improved their ability to appropriately accelerate their eyes at pursuit initiation (Dash and Thier, 2013) or more rapidly estimated RS by shifting their priors towards that target speed (Darlington et al., 2017) resulting in a different retinal image state evolution compared to simulations. In contrast, de Brouwer et al. (2002b) randomized the trial-by-trial target motion using a wide range of possible position steps and velocity shifts. This experimental paradigm was believed to minimize the influence of learning and anticipation and emphasize the visually driven aspects of saccadic decision making,

providing a more ideal dataset to evaluate the model against, which qualitatively matches their behavioural data. Future studies may adapt/extend a similar memory pathway as developed by Orban de Xivry et al. (2013) to properly investigate saccadic decision making during memory-guided pursuit behaviours.

The model also omits the weak influence of PE on pursuit performance. For a given target velocity, initial pursuit acceleration also depends on its initial position error (Lisberger and Westbrook, 1985). Similarly, position error also influences pursuit deceleration and termination at motion offset (Pola and Wyatt, 2001). More recently, it has been shown that position error during steady-state pursuit can have a direct influence on the pursuit trajectory (Blohm et al., 2005). However, these influences only slightly contribute to the variability in pursuit response, whereas the sources of variability accounted in this model, sensory noise and trial-by-trial variability in pursuit gain, seem to have a more dominating influence (Lisberger and Medina, 2015; Osborne et al., 2005). Thus, we believe our simulations accurately reflect the magnitude of visually guided pursuit variability and the omission of a position error input to the pursuit system is minor.

Finally, our model makes no attempt to characterize the evolution of sensory and decision signals during saccade execution. It has been shown that visual acuity is reduced around the time of a saccade, a phenomenon known as saccade suppression (Krekelberg, 2010). The behavioural effect correlates with a suppression of neural activity in visual cortical areas (Bremmer et al., 2009). Saccade suppression has been successfully modelled as a consequence of optimal sensorimotor estimation in the face of signal-dependent noise and sensorimotor delay (Crevecoeur and Kording, 2017). However, we consider this outside the scope of our study since we emphasize investigating the decision mechanism leading to a saccade, not the subsequent sensory consequences of saccade execution.

Generalizability of Model

A major feature of this decision mechanism is the generalizability of saccade confidence as a decision variable compared to the previously hypothesized time-to-foveation parameter (de Brouwer et al., 2002b). Recall that time-to-foveation is defined as $-\frac{PE(t)}{RS(t)}$, which grows to infinity in magnitude as RS approaches zero. Thus, although the parameter correlates with saccade behaviour after an abrupt change in target motion such as in step-ramp trajectories, it is unsuitable as an actual decision variable implemented in the brain. In contrast, the saccade decision mechanism proposed here can explain saccade trigger to both moving and stationary targets.

Another feature of this model is the plausible generalizations that can be made to describe two-dimensional visual tracking compared to the time-to-foveation parameter. The concept behind time-to-foveation is based on the linear extrapolation and intersection of the eye and target trajectories in time, which does not necessarily have an intersection point in two-dimensional tracking. In our framework, a similar saccade confidence estimator that computes the log-probability ratio that the target is above vs below the fovea could be employed to account for vertical and oblique saccade trigger. While conceptually simple, this extension is suboptimal since it implies a loss of covariance information when considering the uncertainty in horizontal and vertical position error independently. A more sophisticated extension speculates that the probability ratio computations underlying the estimation of saccade confidence are implemented through distance dependent inhibition in topographic representations of position error (which would account covariance), similar to proposed dynamic neural field models of saccade generation (Quinton and Goffart, 2018; Trappenberg et al., 2001). Thus, while our current model is constrained to horizontal tracking, there are plausible methods of generalizing the model to account for two-dimensional tracking that merit further investigation.

Neurophysiological Implementation

Our model normatively outlines the computational steps underlying saccadic decisions, which has implications on the signals and connectivity of its neural mechanism. Firstly, the model suggests that motion and position information must converge in a predictive position error estimate which informs the saccade decision process. In macaques, this motion information is likely supplied by middle temporal area (MT) since electrical stimulation shifts saccade amplitudes according to the preferred motion direction of the stimulation site and influences saccade latency in a manner dependent on the trajectory of target motion (Groh et al., 1997). Position information is likely supplied by the superior colliculus (SC), as the spatial locus of activity in the SC correlates with position error during pursuit (Krauzlis et al., 2000) and inactivation of the rostral SC (corresponding to foveal position errors) results in stable eye position offsets during pursuit (Hafed et al., 2008). The frontal eye fields (FEF), characterized as a prediction map for oculomotor control (Crapse and Sommer, 2008), receives motion information from area MT (Ungerleider and Desimone, 1986) and position information from the superior colliculus (Lynch et al., 1994). Various neuronal subpopulations in the pursuit region of FEF have been shown to carry the necessary position and velocity signals for predictive saccadic decision making (Bakst et al., 2017). The lateral intraparietal area (LIP) is also implicated in position prediction, as repetitive transcranial magnetic stimulation suppresses the shifted position percept reported in the flash grab illusion (Edwards et al., 2017). Similarly, predictive eye position signals have been decoded from the ventral intraparietal area during pursuit (Dowiasch et al., 2016), which may also inform predicted position error. Thus, the computation of predicted position error is likely implemented through a distributed network of oculomotor regions.

Secondly, our model suggests neural correlates that integrate predicted PE over time that can trigger saccades upon threshold crossing. Neuronal activity in LIP during perceptual

decision making tasks is consistent with temporal accumulation of evidence supporting a saccade to its movement field (Huk and Shadlen, 2005). In a motion discrimination task, LIP activity predicted monkey's subsequent choice, and the rate of rise in activity correlates with the relative strength of the motion evidence (Shadlen and Newsome, 2001). Additionally, the time that LIP neurons reach a threshold firing rate predicts decision time (Roitman and Shadlen, 2002). Furthermore, during decision tasks based on probabilistic expectations of reward, LIP activity was consistent with temporal accumulation of expected reward (Platt and Glimcher, 1999). Similarly, neuronal activity in the saccade region of FEF is predictive of choice and latency consistent with the decision models of evidence accumulation to a fixed threshold (Hanes and Schall, 1996). Furthermore, the saccade and pursuit subregions of FEF have overlapping projections to the caudate nucleus (Cui et al., 2003) and models suggest this corticostriatal pathway terminating in the superior colliculus is capable of reading out threshold crossing to trigger saccades (Lo and Wang, 2006). Although further investigation targeting saccade decision signals during pursuit are needed, similar oculomotor networks may be responsible for both prediction and confidence accumulation in this normative decision mechanism.

Conclusion

Our model of saccade decision making during pursuit elegantly handles the constraints of delay and signal-dependent noise in the oculomotor system while reproducing known trends in saccade occurrence and latency across a range of target motion trajectories. The model illustrates how continuously controlled orienting movements like pursuit can be programmed directly from sensory estimates, while discretely triggered reorienting movements like saccades employ a second stage of evidence accumulation to determine if/when they should be executed. We suggest that this framework of prediction and confidence estimation represents a fundamental principle in stochastic decision making and sensorimotor coordination.

Acknowledgements

This work was supported by the National Sciences and Engineering Research Council (NSERC, Canada) and the Canada Foundation for Innovation (CFI). JDC would like to thank Brandon Caie, Alex Göttker and Julia Morris for valuable discussions and feedback.

References

Bahill AT, Clark MR, Stark LW. 1975. The Main Sequence, A Tool for Studying Human Eye Movements. *Math Biosci* **24**:191–204. doi:10.1016/0025-5564(75)90075-9

Bakst L, Fleuriet J, Mustari MJ. 2017. Temporal Dynamics of Retinal and Extraretinal Signals in the FEFsem during Smooth Pursuit Eye Movements. *J Neurophysiol* jn.00786.2016. doi:10.1152/jn.00786.2016

Beck JM, Ma WJ, Pitkow X, Latham PE, Pouget A. 2012. Not Noisy, Just Wrong: The Role of Suboptimal Inference in Behavioral Variability. *Neuron* **74**:30–39. doi:10.1016/j.neuron.2012.03.016

Bennett SJ, Orban de Xivry J-J, Barnes GR, Lefèvre P. 2007. Target acceleration can be extracted and represented within the predictive drive to ocular pursuit. *J Neurophysiol* **98**:1405–1414. doi:10.1152/jn.00132.2007

Bieg HJ, Chuang LL, Bülthoff HH, Bresciani JP. 2015. Asymmetric saccade reaction times to smooth pursuit. *Exp Brain Res* **233**:2527–2538. doi:10.1007/s00221-015-4323-8

Blohm G, Missal M, Lefèvre P. 2005. Direct evidence for a position input to the smooth pursuit system. *J Neurophysiol* **94**:712–721. doi:10.1152/jn.00093.2005

Blohm G, Optican LM, Lefèvre P. 2006. A model that integrates eye velocity commands to keep track of smooth eye displacements. *J Comput Neurosci* **21**:51–70. doi:10.1007/s10827-006-7199-6

Bremmer F, Kubischik M, Hoffmann K-P, Krekelberg B. 2009. Neural Dynamics of Saccadic Suppression. *J Neurosci* **29**:12374–12383. doi:10.1523/JNEUROSCI.2908-09.2009

Carpenter RH, Reddi B. 2001. Reply - Putting noise into neurophysiological models of simple decision making. *Nat Neurosci* **4**:336–337. doi:10.1038/85956

Chang C-J, Jazayeri M. 2018. Integration of speed and time for estimating time to contact. *Proc Natl Acad Sci* **115**:201713316. doi:10.1073/pnas.1713316115

Chen J, Valsecchi M, Gegenfurtner KR. 2017. Attention is allocated closely ahead of the target during smooth pursuit eye movements: Evidence from EEG frequency tagging. *Neuropsychologia* **102**:206–216. doi:10.1016/j.neuropsychologia.2017.06.024

Crapse TB, Sommer MA. 2008. The frontal eye field as a prediction map. *Prog Brain Res* **171**:383–390. doi:10.1016/S0079-6123(08)00656-0

Crevecoeur F, Kording KP. 2017. Saccadic suppression as a perceptual consequence of efficient sensorimotor estimation. *Elife* **6**. doi:10.7554/eLife.25073

Cui D-MM, Yan Y-JJ, Lynch JC. 2003. The pursuit subregion of the frontal eye field projects to the caudate nucleus in monkeys. *J Neurophysiol* **89**:2678–2684. doi:10.1152/jn.00501.2002

Darlington TR, Tokiyama S, Lisberger SG. 2017. Control of the strength of visual-motor transmission as the mechanism of rapid adaptation of priors for Bayesian inference in smooth pursuit eye movements. *J Neurophysiol* **118**:1173–1189. doi:10.1152/jn.00282.2017

Dash S, Thier P. 2013. Smooth pursuit adaptation (SPA) exhibits features useful to compensate changes in the properties of the smooth pursuit eye movement system due to usage. *Front*

Syst Neurosci **7**:67. doi:10.3389/fnsys.2013.00067

de Brouwer S, Missal M, Barnes GR, Lefèvre P. 2002a. Quantitative analysis of catch-up saccades during sustained pursuit. *J Neurophysiol* **87**:1772–80. doi:10.1152/jn.00621.2001

de Brouwer S, Missal M, Lefèvre P. 2001. Role of Retinal Slip in the Prediction of Target Motion During Smooth and Saccadic Pursuit. *J Neurophysiol* **86**:550–558.

de Brouwer S, Yuksel D, Blohm G, Missal M, Lefèvre P. 2002b. What Triggers Catch-Up Saccades During Visual Tracking? *J Neurophysiol* **87**:1646–1650. doi:10.1152/jn.00432.2001

Dowiasch S, Blohm G, Bremmer F, Foxe J. 2016. Neural correlate of spatial (mis-)localization during smooth eye movements. *Eur J Neurosci* **44**:1846–1855. doi:10.1111/ejn.13276

Edwards G, Paeye C, Marque P, VanRullen R, Cavanagh P. 2017. Predictive position computations mediated by parietal areas: TMS evidence. *Neuroimage* **153**:49–57. doi:10.1016/j.neuroimage.2017.03.043

Faisal AA, Selen LPJ, Wolpert DM. 2008. Noise in the nervous system. *Nat Rev Neurosci* **9**:292–303. doi:10.1038/nrn2258

Forstmann BU, Ratcliff R, Wagenmakers E-J. 2016. Sequential Sampling Models in Cognitive Neuroscience: Advantages, Applications, and Extensions. *Annu Rev Psychol* **67**:641–666. doi:10.1146/annurev-psych-122414-033645

Goffart L. 2009. Saccadic Eye MovementsEncyclopedia of Neuroscience. pp. 437–444. doi:10.1016/0042-6989(77)90087-6

Gold JI, Shadlen MN. 2007. The Neural Basis of Decision Making. *Annu Rev Neurosci* **30**:535–574. doi:10.1146/annurev.neuro.29.051605.113038

Gold JI, Shadlen MN. 2001. Neural computations that underlie decisions about sensory stimuli. *Trends Cogn Sci* **5**:10–16. doi:10.1016/S1364-6613(00)01567-9

Goossens HHLM, van Opstal AJ. 2012. Optimal control of saccades by spatial-temporal activity patterns in the monkey superior colliculus. *PLoS Comput Biol* **8**. doi:10.1371/journal.pcbi.1002508

Groh JM, Born RT, Newsome WT. 1997. How is a sensory map read Out? Effects of microstimulation in visual area MT on saccades and smooth pursuit eye movements. *J Neurosci* **17**:4312–4330.

Guan Y, Eggert T, Bayer O, Büttner U. 2005. Saccades to stationary and moving targets differ in the monkey. *Exp Brain Res* **161**:220–232. doi:10.1007/s00221-004-2070-3

Hafed ZM, Goffart L, Krauzlis RJ. 2008. Superior Colliculus Inactivation Causes Stable Offsets in Eye Position during Tracking. *J Neurosci* **28**:8124–8137. doi:10.1523/JNEUROSCI.1317-08.2008

Hanes DP, Schall JD. 1996. Neural Control of Voluntary Movement Initiation. *Science (80-)* **274**:427–430.

Hanks TD, Summerfield C. 2017. Perceptual Decision Making in Rodents, Monkeys, and Humans. *Neuron*. doi:10.1016/j.neuron.2016.12.003

Harris CM, Wolpert DM. 2006. The main sequence of saccades optimizes speed-accuracy

trade-off. *Biol Cybern* **95**:21–29. doi:10.1007/s00422-006-0064-x

Harris CM, Wolpert DM. 1998. Signal-dependent noise determines motor planning. *Nature* **394**:780–784. doi:10.1038/29528

Hu X, Jiang H, Gu C, Li C, Sparks DL. 2007. Reliability of oculomotor command signals carried by individual neurons. *Proc Natl Acad Sci U S A* **104**:8137–42. doi:10.1073/pnas.0702799104

Huk AC, Shadlen MN. 2005. Neural Activity in Macaque Parietal Cortex Reflects Temporal Integration of Visual Motion Signals during Perceptual Decision Making. *J Neurosci* **25**:10420–10436. doi:10.1523/JNEUROSCI.4684-04.2005

Izawa J, Rane T, Donchin O, Shadmehr R. 2008. Motor adaptation as a process of reoptimization. *J Neurosci* **28**:2883–91. doi:10.1523/JNEUROSCI.5359-07.2008

Jürgens R, Becker W, Kornhuber HH. 1981. Natural and drug-induced variations of velocity and duration of human saccadic eye movements: evidence for a control of the neural pulse generator by local feedback. *Biol Cybern* **39**:87–96.

Kalman RE, Bucy RS. 1961. New Results in Linear Filtering and Prediction Theory. *J Basic Eng* **83**:95. doi:10.1115/1.3658902

Keller EL, Heinen SJ. 1991. Generation of smooth-pursuit eye movements: neuronal mechanisms and pathways. *Neurosci Res* **11**:79–107. doi:10.1016/0168-0102(91)90048-4

Khan AZ, Lefèvre P, Heinen SJ, Blohm G. 2010. The default allocation of attention is broadly ahead of smooth pursuit. *J Vis* **10**:7. doi:10.1167/10.13.7

Kowler E, Anderson E, Dosher B, Blaser E. 1995. The role of attention in the programming of saccades. *Vision Res* **35**:1897–1916. doi:10.1016/0042-6989(94)00279-U

Krauzlis RJ. 2004. Recasting the smooth pursuit eye movement system. *J Neurophysiol* **91**:591–603. doi:10.1152/jn.00801.2003

Krauzlis RJ, Basso MA, Wurtz RH. 2000. Discharge properties of neurons in the rostral superior colliculus of the monkey during smooth-pursuit eye movements. *J Neurophysiol* **84**:876–91.

Krauzlis RJ, Lisberger SG. 1994. A model of visually-guided smooth pursuit eye movements based on behavioral observations. *J Comput Neurosci* **1**:265–283. doi:10.1007/BF00961876

Krauzlis RJ, Miles FA. 1996. Transitions between pursuit eye movements and fixation in the monkey: dependence on context. *J Neurophysiol* **76**:1622–1638.

Krekelberg B. 2010. Saccadic suppression. *Curr Biol* **20**:R228-9. doi:10.1016/j.cub.2009.12.018

Lisberger SG, Medina JF. 2015. How and why neural and motor variation are related. *Curr Opin Neurobiol* **33**:110–6. doi:10.1016/j.conb.2015.03.008

Lisberger SG, Westbrook LE. 1985. Properties of visual inputs that initiate horizontal smooth pursuit eye movements in monkeys. *J Neurosci* **5**:1662–1673. doi:10.1523/JNEUROSCI.05-06-01662.1985

Lo C-C, Wang X-J. 2006. Cortico-basal ganglia circuit mechanism for a decision threshold in reaction time tasks. *Nat Neurosci* **9**. doi:10.1038/nn1722

Lynch JC, Hoover JE, Strick PL. 1994. Input to the primate frontal eye field from the substantia nigra, superior colliculus, and dentate nucleus demonstrated by transneuronal transport. *Exp Brain Res* **100**:181–186.

Maunsell JHR, Van Essen DC. 1983. Functional Properties of Neurons in Middle Temporal Visual Area of the Macaque Monkey. I. Selectivity for Stimulus Direction, Speed, and Orientation. *J Neurophysiol* **49**.

Nover H, Anderson CH, DeAngelis GC. 2005. A Logarithmic, Scale-Invariant Representation of Speed in Macaque Middle Temporal Area Accounts for Speed Discrimination Performance. *J Neurosci* **25**:10049–10060. doi:10.1523/JNEUROSCI.1661-05.2005

Orban de Xivry J-J, Coppe S, Blohm G, Lefèvre P. 2013. Kalman Filtering Naturally Accounts for Visually Guided and Predictive Smooth Pursuit Dynamics. *J Neurosci* **33**:17301–17313. doi:10.1523/JNEUROSCI.2321-13.2013

Orban de Xivry J-J, Lefèvre P. 2007. Saccades and pursuit: two outcomes of a single sensorimotor process. *J Physiol* **584**:11–23. doi:10.1113/jphysiol.2007.139881

Osborne LC. 2011. Computation and physiology of sensory-motor processing in eye movements. *Curr Opin Neurobiol* **21**:623–628. doi:10.1016/j.conb.2011.05.023

Osborne LC, Hohl SS, Bialek W, Lisberger SG. 2007. Time course of precision in smooth-pursuit eye movements of monkeys. *J Neurosci* **27**:2987–2998. doi:10.1523/JNEUROSCI.5072-06.2007

Osborne LC, Lisberger SG. 2009. Spatial and Temporal Integration of Visual Motion Signals for Smooth Pursuit Eye Movements in Monkeys 2013–2025. doi:10.1152/jn.00611.2009.

Osborne LC, Lisberger SG, Bialek W. 2005. A sensory source for motor variation. *Nature* **437**:412–416. doi:10.1038/nature03961

Platt ML, Glimcher PW. 1999. Neural correlates of decision variables in parietal cortex. *Nature* **400**:233–238. doi:10.1038/22268

Pola J, Wyatt HJ. 2001. The role of target position in smooth pursuit deceleration and termination. *Vision Res* **41**:655–669. doi:10.1016/S0042-6989(00)00280-7

Poletti M, Rucci M, Carrasco M. 2017. Selective attention within the foveola. *Nat Neurosci*. doi:10.1038/nn.4622

Pouget A, Drugowitsch J, Kepecs A. 2016. Confidence and certainty: distinct probabilistic quantities for different goals. *Nat Neurosci* **19**:366–374. doi:10.1038/nn.4240

Price NS, Ibbotson MR, Ono S, Mustari MJ. 2005. Rapid processing of retinal slip during saccades in macaque area MT. *J Neurophysiol* **94**:235–246. doi:10.1152/jn.00041.2005

Quinet J, Goffart L. 2015. Does the Brain Extrapolate the Position of a Transient Moving Target? *J Neurosci* **35**:11780–11790. doi:10.1523/JNEUROSCI.1212-15.2015

Quinton J-C, Goffart L. 2018. A unified dynamic neural field model of goal directed eye movements. *Conn Sci* **30**:20–52. doi:10.1080/09540091.2017.1351421

Rashbass C. 1961. The relationship between saccadic and smooth tracking eye movements. *J Physiol* **159**:326–338. doi:10.1016/0196-9781(92)90172-Y

Ratcliff R. 2001. Putting Noise into Neurophysiological Models of Simple Decision Making. *Nat*

Neurosci. doi:10.1038/85960

Regan D, Gray R. 2000. Visually guided collision avoidance and collision achievement. *Trends Cogn Sci* **4**:99–107. doi:10.1016/S1364-6613(99)01442-4

Robinson DA. 1973. Models of the saccadic eye movement control system. *Biol Cybern* **14**:71–83. doi:10.1007/BF00288906

Roitman JD, Shadlen MN. 2002. Response of neurons in the lateral intraparietal area during a combined visual discrimination reaction time task. *J Neurosci* **22**:9475–9489. doi:10.1016/S0377-2217(02)00363-6

Schall JD. 2001. Neural basis of deciding, choosing and acting. *Nat Rev Neurosci* **2**:33–42. doi:10.1038/35049054

Schall JD. 2000. Decision making: From sensory evidence to a motor command. *Curr Biol* **10**. doi:10.1016/S0960-9822(00)00504-2

Schreiber C, Missal M, Lefèvre P. 2006. Asynchrony between position and motion signals in the saccadic system. *J Neurophysiol* **95**:960–9. doi:10.1152/jn.00315.2005

Scudder CA. 1988. A new local feedback model of the saccadic burst generator. *J Neurophysiol* **59**:1455–75.

Shadlen MN, Newsome WT. 2001. Neural Basis of a Perceptual Decision in the Parietal Cortex (Area LIP) of the Rhesus Monkey. *J Neurophysiol* **86**:1916–1936. doi:10.3410/f.1001494.23207

Sparks DL. 1986. Translation of sensory signals into commands for control of saccadic eye movements: role of primate superior colliculus. *Physiol Rev* **66**:118–171.

Stein RB, Gossen ER, Jones KE. 2005. Neuronal variability: Noise or part of the signal? *Nat Rev Neurosci*. doi:10.1038/nrn1668

Tavassoli A, Ringach DL. 2009. Dynamics of Smooth Pursuit Maintenance. *J Neurophysiol* **102**:110–118. doi:10.1152/jn.91320.2008

Todorov E. 2005. Stochastic optimal control and estimation methods adapted to the noise characteristics of the sensorimotor system. *Neural Comput* **17**:1084–1108. doi:10.1162/0899766053491887

Trappenberg TP, Dorris MC, Munoz DP, Klein RM. 2001. A model of saccade initiation based on the competitive integration of exogenous and endogenous signals in the superior colliculus. *J Cogn Neurosci* **13**:256–271. doi:10.1162/089892901564306

Tresilian JR. 1995. Perceptual and cognitive processes in time-to-contact estimation: analysis of prediction-motion and relative judgment tasks. *Percept Psychophys* **57**:231–245. doi:10.3758/BF03206510

Ungerleider LG, Desimone R. 1986. Cortical connections of visual area MT in the macaque. *J Comp Neurol* **248**:190–222. doi:10.1002/cne.902480204

van Beers RJ. 2007. The sources of variability in saccadic eye movements. *J Neurosci* **27**:8757–8770. doi:10.1523/JNEUROSCI.2311-07.2007

van Beers RJ, Baraduc P, Wolpert DM. 2002. Role of uncertainty in sensorimotor control. *Philos Trans R Soc B Biol Sci* **357**:1137–1145. doi:10.1098/rstb.2002.1101

Van Gisbergen JAM, Robinson DA, Gielen S. 1981. A quantitative analysis of generation of saccadic eye movements by burst neurons. *J Neurophysiol* **45**:417–42.

Van Gompel RPG, Fischer MH, Murray WS, Hill RL. 2007. Eye-movement research. An overview of current and past developmentsEye Movements. Elsevier. pp. 1–28. doi:10.1016/B978-008044980-7/50003-3

Wald A, Wolfowitz J. 1948. Optimum Character of the Sequential Probability Ratio Test. *Source Ann Math Stat* **19**:326–339.

Wolpert DM, Landy MS. 2012. Motor control is decision-making. *Curr Opin Neurobiol*. doi:10.1016/j.conb.2012.05.003

Zhao M, Gersch TM, Schnitzer BS, Dosher BA, Kowler E. 2012. Eye movements and attention: The role of pre-saccadic shifts of attention in perception, memory and the control of saccades. *Vision Res* **74**:40–60. doi:10.1016/j.visres.2012.06.017

Kalman Filter Parameters	**Value**
Additive noise, R	$\begin{bmatrix} 0.1 & 0 & 0 \\ 0 & 1 & 0 \\ 0 & 0 & 50 \end{bmatrix}$
Multiplicative noise, D	$\begin{bmatrix} 1 & 0 & 0 \\ 0 & 1 & 0 \\ 0 & 0 & 1 \end{bmatrix}$
Expected variability, Q	$\begin{bmatrix} 0.1 & 0 & 0 \\ 0 & 1 & 0 \\ 0 & 0 & 30 \end{bmatrix}$
Internal process noise, Ω	$\begin{bmatrix} 0.01 & 0 & 0 \\ 0 & 0.3 & 0 \\ 0 & 0 & 10 \end{bmatrix}$

Table 1: Parameters used for Kalman filtering in sensory pathway.

Figure Captions

Figure 1: Global overview of model. Sensory Pathway (blue): Visual sensory signals (position error, retinal slip, retinal acceleration) are delayed by 70 ms, corrupted by signal-dependent noise, estimated through Kalman filtering (Equations 1-8), then linearly extrapolated to compensate for delay (Equations 9-12). Decision Pathway (purple): Predicted position error is used to compute the probability ratio of the target left & right of the fovea (Equation 13), which is temporally (leaky) integrated (Equation 14), and triggers saccades after threshold crossing. Motor pathway (red): Described further in Figure 2.

Figure 2: Motor Processing Pathways. Pursuit (blue): The predictive estimate of retinal slip is subject to a linear gain function (G), a second-order filter (H), a variable gain element (A), then leaky integration with a 100ms time constant (Equations 15-17). Saccade (green): The input to the saccade pathway is the predictive estimate of position error. The saccade velocity command produced by a pulse generator (PG, Equation 18), which is integrated (resettable integrator, RI) to provide negative feedback ensuring the appropriate saccade amplitude. Final common motor pathway (red): The sum of the saccade and pursuit velocity commands are sent to the eye plant and a parallel integration pathway whose output is also sent to the eye plant enabling stable eccentric eye positions. The eye plant is modelled as a second-order overdamped linear system.

Figure 3: Schematic of saccade confidence computation. (A) Probabilistic representation of predicted position error with a mean of 2 deg and uncertainty of 0.75^2 (blue) and 2^2 (red) deg^2. (C) Temporal evolution of saccade confidence without noise based on predicted position error estimates from A. (B&D) Same format for a predicted position error of 4 deg with an uncertainty of 0.75^2 (blue) and 2^2 (red) deg^2.

Figure 4: Single trial simulations comparing oculomotor responses to a target that steps 4 degrees then moves at 20 deg/s (red), -20 deg/s (blue) or zero deg/s (grey). (A) Target and simulated eye trajectory over time. When the target recrosses the initial fixation position in 200 ms (blue), a saccade was not triggered, while the gray and red traces led to saccade trigger. (B) The sensory estimate of position error over time in response to each target trajectory. (C) The sensory estimate of retinal slip over time. (D) The predictive estimate of position error over time. This predictive estimate is used to compute saccade confidence (E) which triggers saccades upon threshold crossing.

Figure 5: Model simulations illustrating saccade proportion (± standard deviation) and mean saccade latency (± standard deviation) as a function of position step size for the two target speeds (|VS|) tested by Bieg et al., 2015. Foveopetal target motion (red) describes trajectories where the velocity shift (VS) and position step are in opposite directions. Foveofugal target motion (green) describes trajectories with velocity shift and position step in the same direction.

Figure 6: Single trial simulations comparing oculomotor responses to step-ramp perturbations during pursuit maintenance at 10 deg/s. The step-ramp consists of a 4 deg step followed by a change in speed of 20 deg/s (red) or -20 deg/s (blue). (A) Target and simulated eye trajectory over time. (B) The sensory estimate of position error over time in response to each target trajectory. (C) The sensory estimate of retinal slip over time. (D) The predictive estimate of position error over time. This predictive estimate is used to compute saccade confidence, (E), which triggers saccades upon threshold crossing.

Figure 7: Sensory conditions (RS and PE) preceding saccade execution in simulations (left) and human behavioural data (de Brouwer et al., 2002, right). Model simulations result in similar sensory conditions prior to the time of saccade execution as observed in behavioural data.

Figure 8: Model simulations (left) reproduce trends in saccade occurrence (above) and latency (below) during steady-state pursuit, as described in behavioural studies (de Brouwer et al., 2002; right). Both simulations and behavioural results show increased saccade latency and decreased saccade occurrence in and around the “smooth zone”, marked in dashed lines (left) and arrows (right).

Figure 9: Influence of increasing position error uncertainty on saccade latency distributions. For negative time-to-foveation (Txt) target trajectories, there is a negligible influence of increased position error uncertainty on saccade latency. When time-to-foveation is between 0 and 400 ms, increasing position error uncertainty leads to an overall reduction in saccade occurrence and bimodal distribution in saccade latency. When time-to-foveation is above 400 ms, an intermediate increase in the variability of saccade latency is predicted.

Figure 1

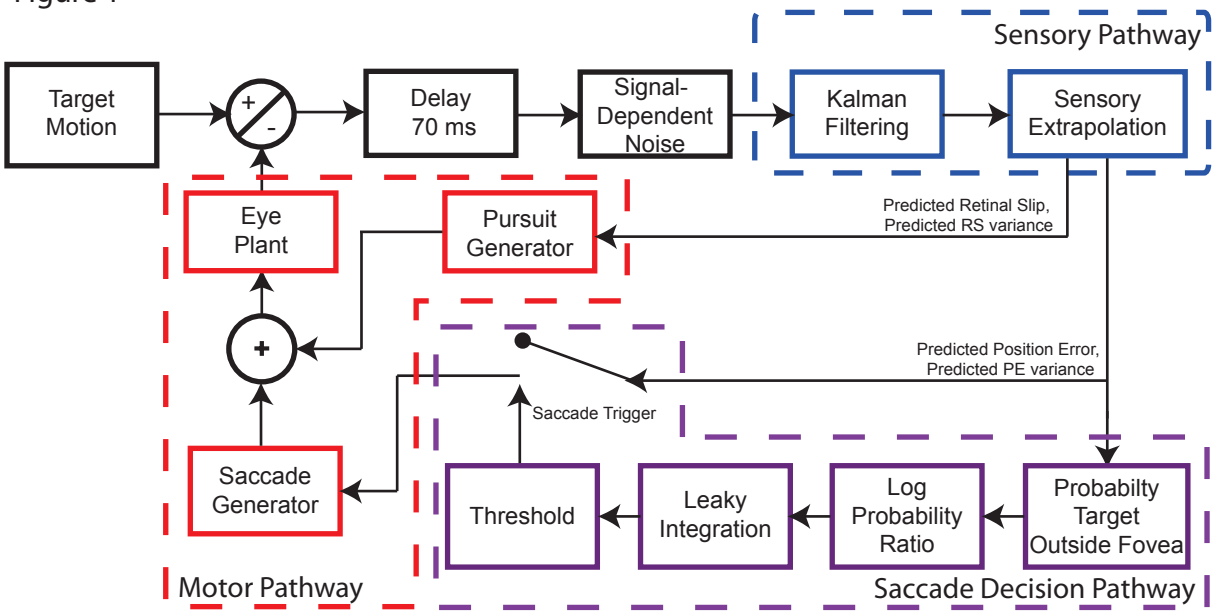
Sensory Pathway
Target Motion
+
-
Delay 70 ms
Signal-Dependent Noise
Kalman Filtering
Sensory Extrapolation
Eye Plant
Pursuit Generator
Predicted Retinal Slip, Predicted RS variance
+
Predicted Position Error, Predicted PE variance
Saccade Trigger
Saccade Generator
Threshold
Leaky Integration
Log Probability Ratio
Probabilty Target Outside Fovea
Motor Pathway
Saccade Decision Pathway

Figure 2

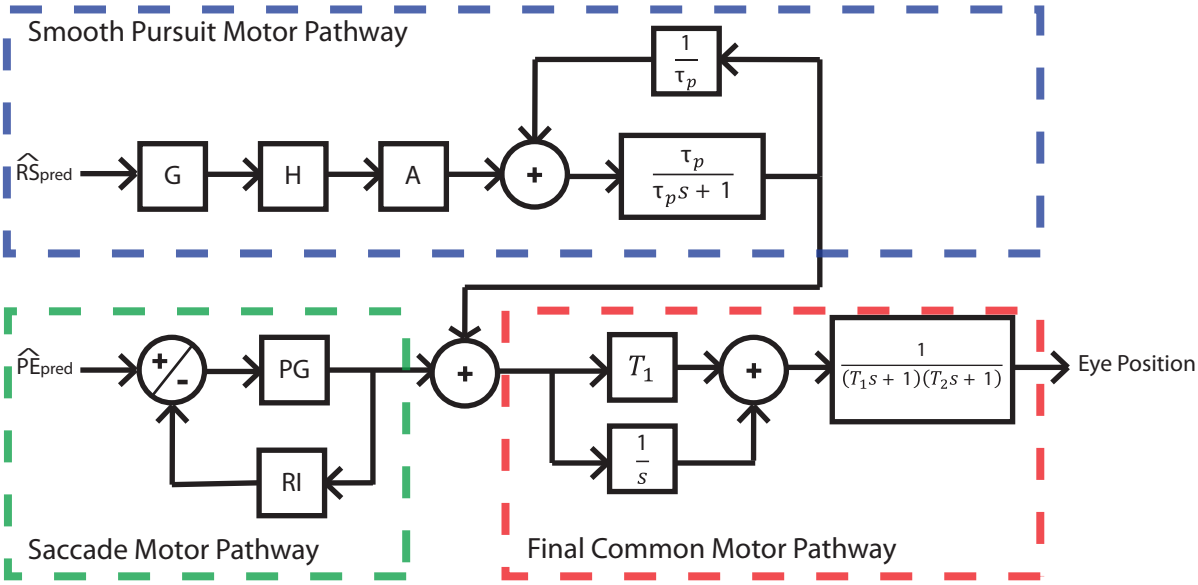
Smooth Pursuit Motor Pathway
$\widehat{RS}_{pred}$
G
H
A
+
$\frac{1}{\tau_p}$
$\frac{\tau_p}{\tau_p s + 1}$
$\widehat{PE}_{pred}$
+
-
PG
RI
+
T_1
+
$\frac{1}{s}$
$\frac{1}{(T_1 s + 1)(T_2 s + 1)}$
Eye Position
Saccade Motor Pathway
Final Common Motor Pathway

Figure 3

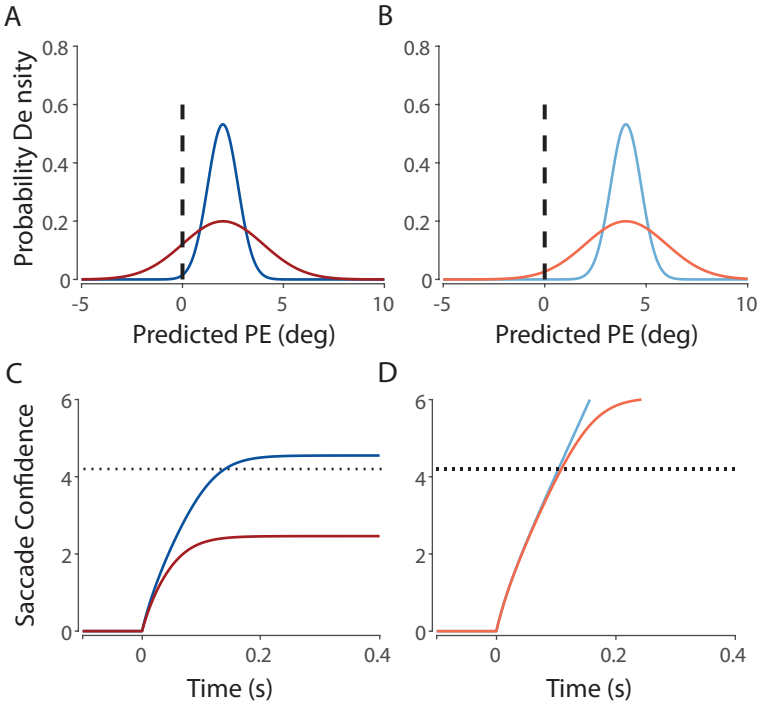
A
B
C
D
Probability Density
0.8
0.6
0.4
0.2
0
-5
0
5
10
Predicted PE (deg)
Saccade Confidence
6
4
2
0
0.2
0.4
Time (s)

Figure 4

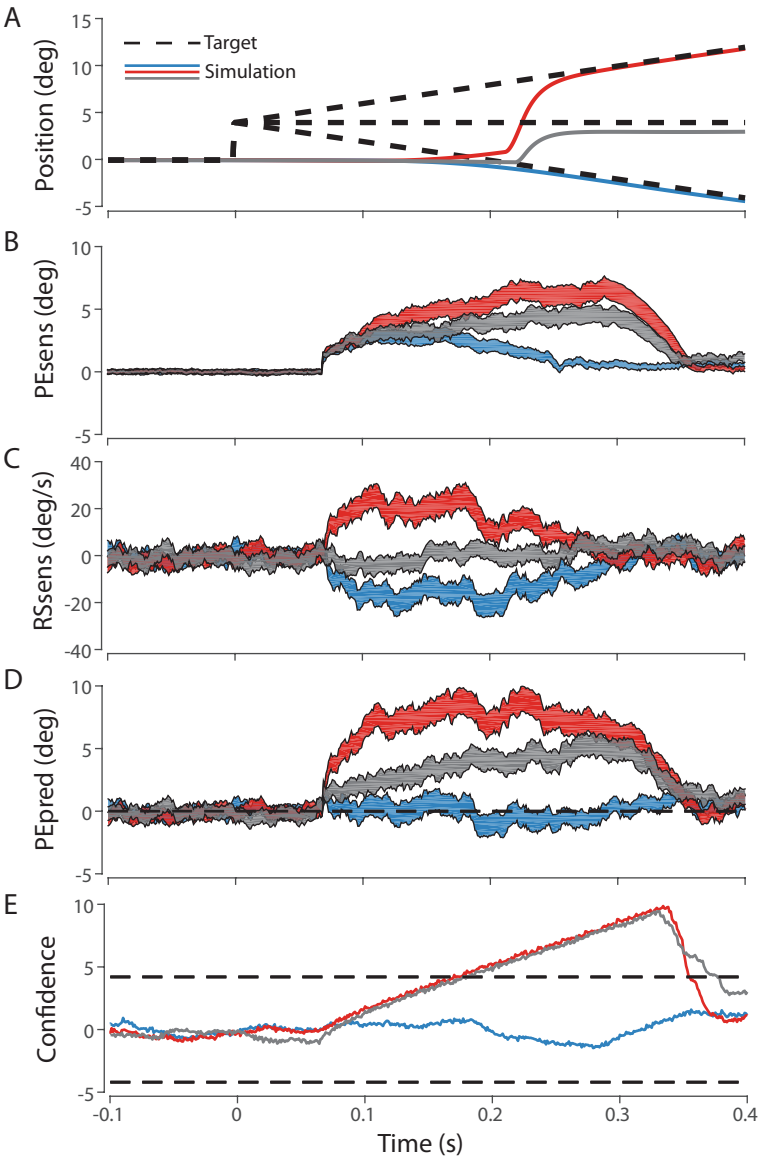
A
Position (deg)
Target
Simulation
B
PEsens (deg)
C
RSsens (deg/s)
D
PEpred (deg)
E
Confidence
Time (s)

Figure 5

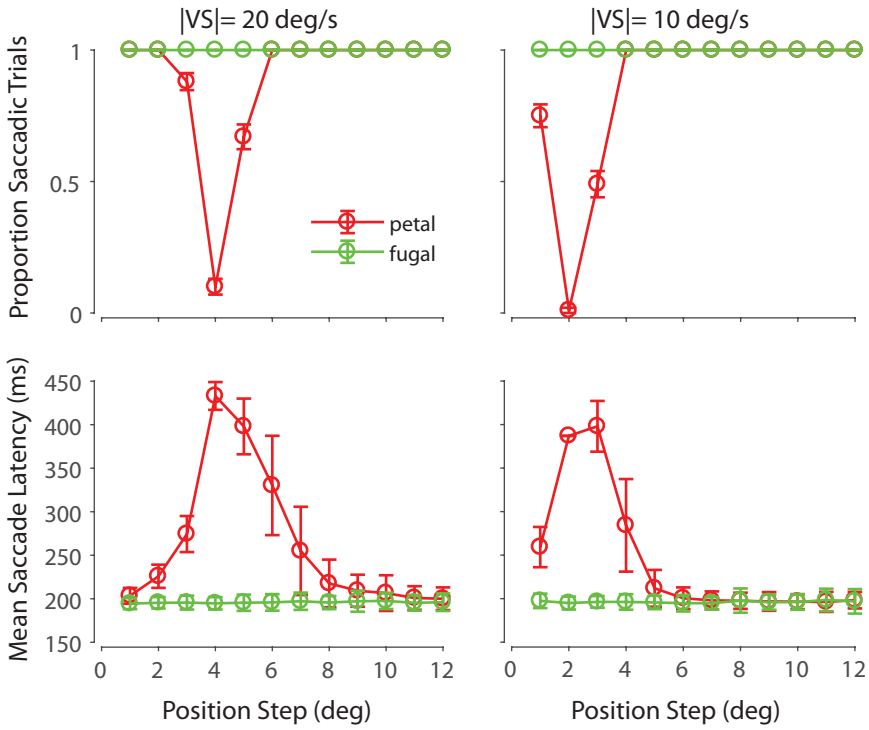
|VS|= 20 deg/s
|VS|= 10 deg/s
Proportion Saccadic Trials
1
0.5
0
petal
fugal
Mean Saccade Latency (ms)
450
400
350
300
250
200
150
0
2
4
6
8
10
12
Position Step (deg)
Position Step (deg)

Figure 6

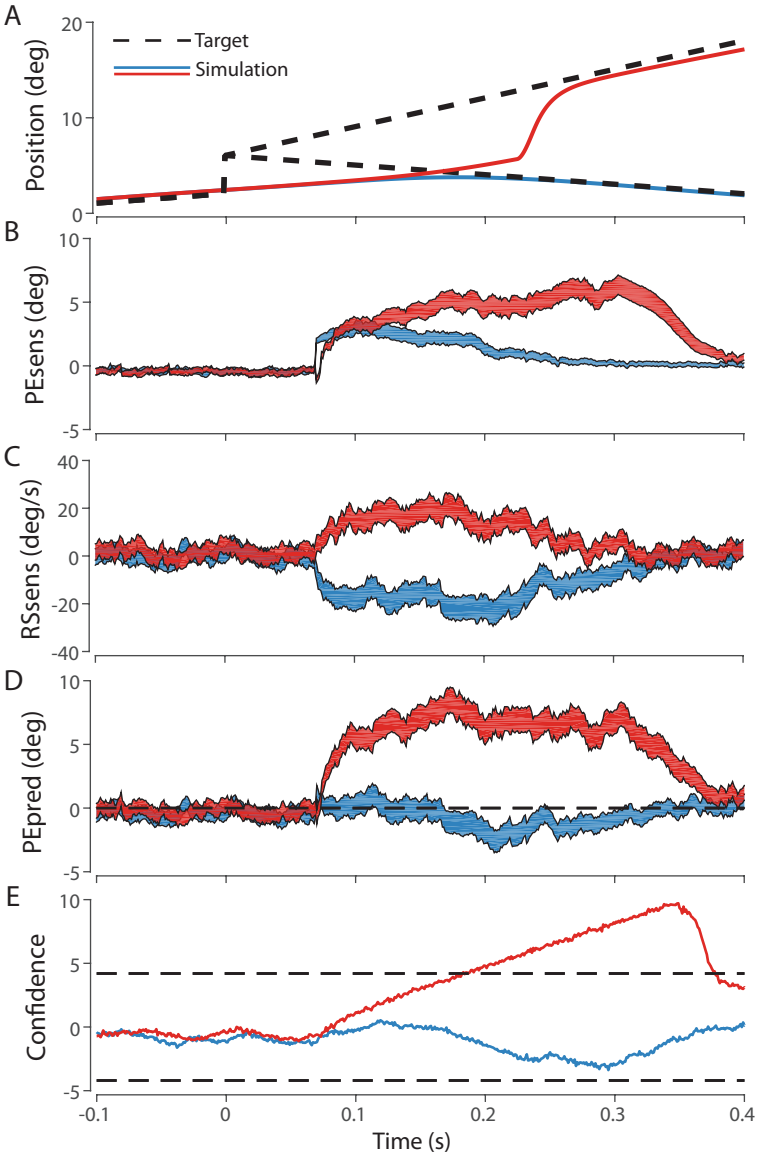
A
Target
Simulation
Position (deg)
20
10
0
B
PEsens (deg)
10
5
0
-5
C
RSsens (deg/s)
40
20
0
-20
-40
D
PEpred (deg)
10
5
0
-5
E
Confidence
10
5
0
-5
-0.1
0
0.1
0.2
0.3
0.4
Time (s)

Figure 7

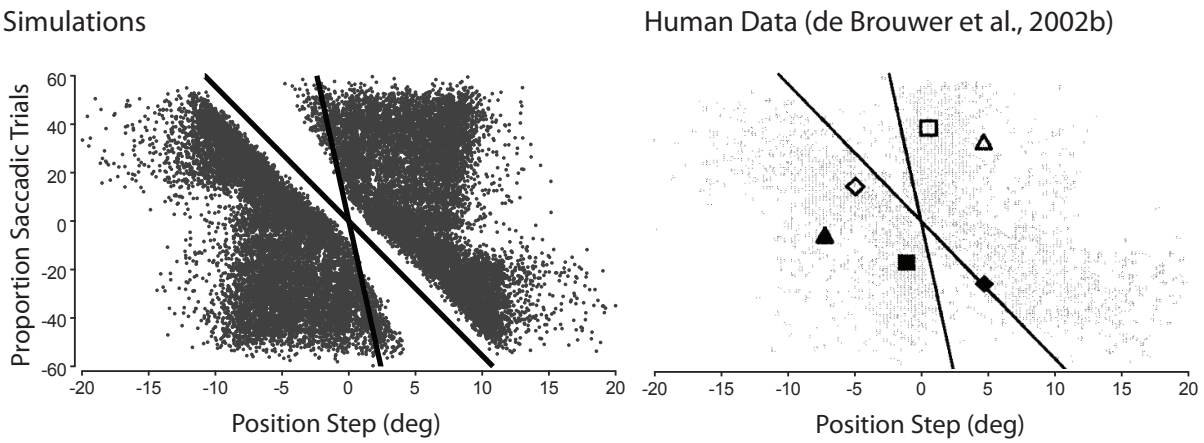
Simulations
Human Data (de Brouwer et al., 2002b)
Proportion Saccadic Trials
60
40
20
0
-20
-40
-60
-20
-15
-10
-5
0
5
10
15
20
Position Step (deg)
Position Step (deg)

Figure 8

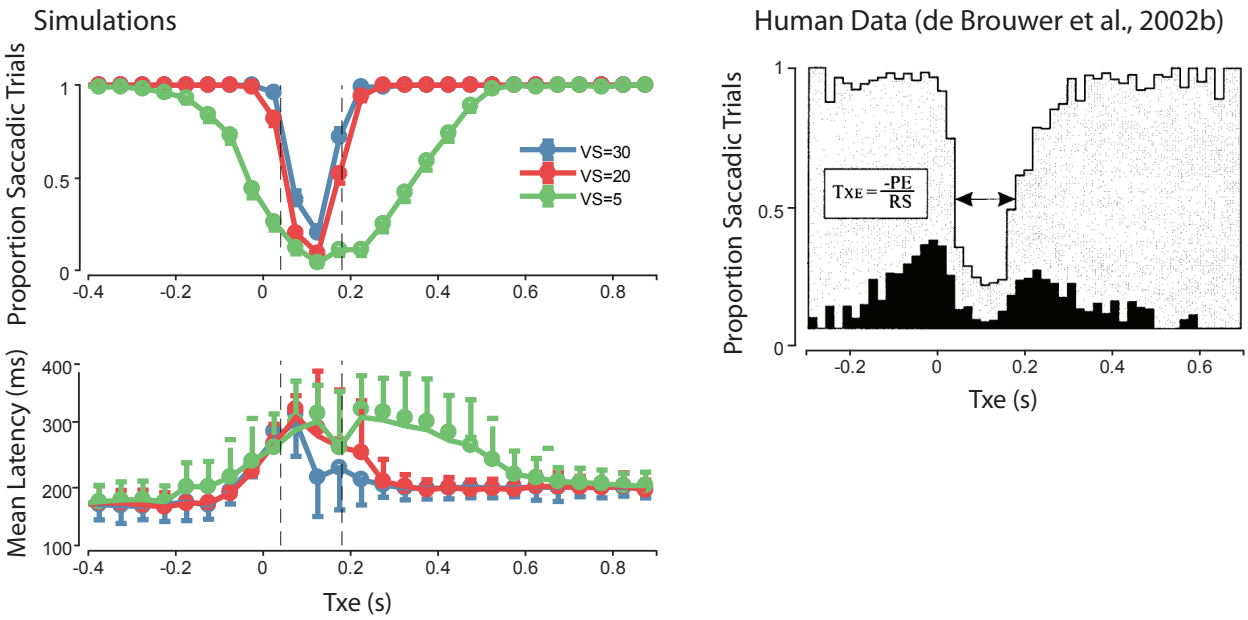
Simulations
Proportion Saccadic Trials
VS=30
VS=20
VS=5
Mean Latency (ms)
Txe (s)
Human Data (de Brouwer et al., 2002b)
Proportion Saccadic Trials
TXE = -PE / RS
Txe (s)

Figure 9

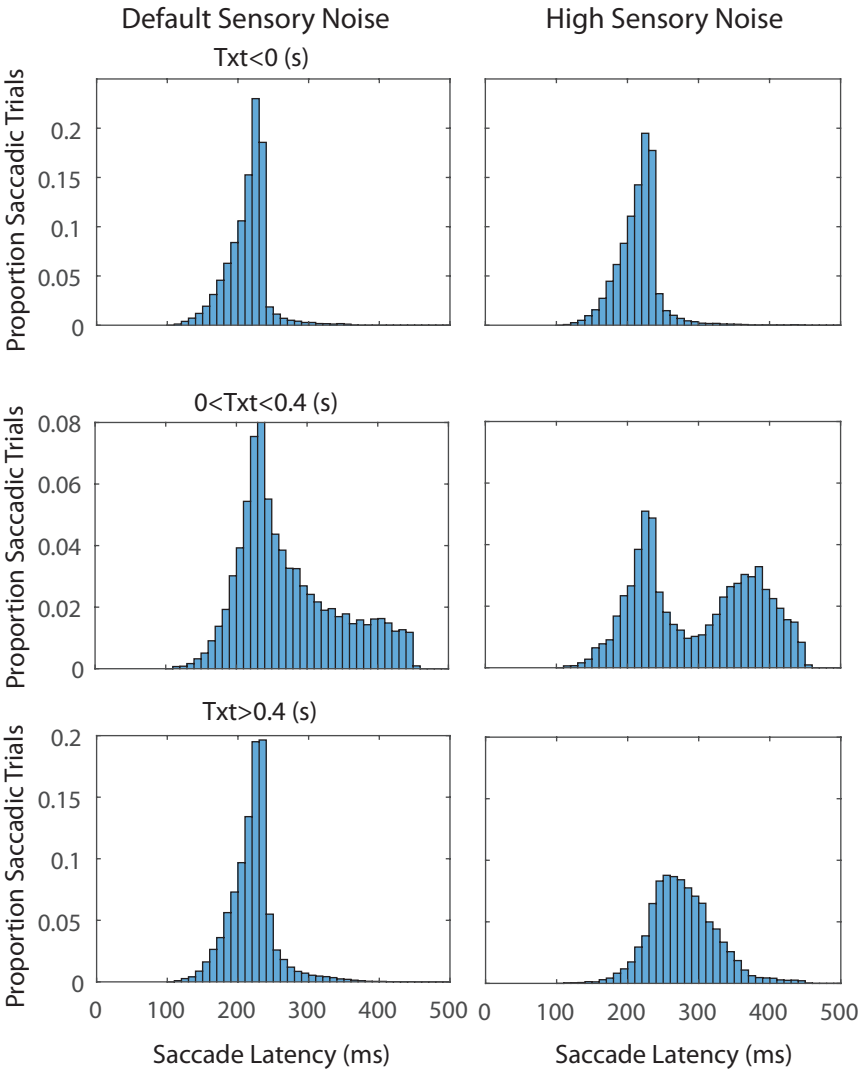
Default Sensory Noise
High Sensory Noise
Txt<0 (s)
0<Txt<0.4 (s)
Txt>0.4 (s)
Proportion Saccadic Trials
0
0.05
0.1
0.15
0.2
0.02
0.04
0.06
0.08
0
100
200
300
400
500
Saccade Latency (ms)